

# Bond order potential for gold

M. Backman<sup>1,2,a</sup>, N. Juslin<sup>3</sup>, and K. Nordlund<sup>1</sup>

<sup>1</sup> Department of Physics, University of Helsinki, P.O. Box 43, 00014 Helsinki, Finland

<sup>2</sup> Department of Materials Science and Engineering, University of Tennessee, Knoxville, 37996 Tennessee, USA

<sup>3</sup> Department of Nuclear Engineering, University of Tennessee, Knoxville, 37996 Tennessee, USA

Received 29 May 2012 / Received in final form 7 August 2012

Published online 17 September 2012 – © EDP Sciences, Società Italiana di Fisica, Springer-Verlag 2012

**Abstract.** We develop an analytic bond order potential for modelling of gold. The bond order formalism includes bond angularity and offers an alternative approach to the embedded atom type potentials frequently used to describe metallic bonding. The advantage of the developed potential is that it can be extended to describe interactions with covalent materials. Experimental and ab initio data of gold properties is used to fit the potential and a good description of bulk and defect properties is achieved. We use the potential to simulate melting of nanoclusters and find that the experimentally observed size dependent melting behaviour is reproduced qualitatively.

## 1 Introduction

The noble metal gold has countless applications in chemistry, electronics, materials science, and medicine and has therefore been studied extensively in both experiments, electronic structure calculations, and atomistic simulations using empirical potentials.

In order to simulate gold and other metals, where bonding depends on local electron density and hence coordination number, many developed potentials include an effective electron density term in addition to pairwise interactions. Examples include gold potentials using the embedded atom model (EAM) [1–4], the glue model [5], the corrected effective medium (MD/MC-CEM) theory [6], and the Cleri-Rosato-type tight binding (TB) potentials [7–9]. Bond directionality has, however, been found to be important in small gold clusters [10], which can explain some of the shortcomings of the aforementioned spherically symmetric potentials in describing for instance surface energies. To solve this problem, gold potentials with angular dependence have been developed in the ReaxFF framework [11,12] and in a potential by Olivier et al. [13].

The strength of “Tersoff-like” analytic bond order potentials [14–17] lies in their ability to describe directional bonds. For this reason they have conventionally been used to model covalently bonded materials. However, Brenner [18] has shown that the Tersoff formalism is in absence of angular terms equivalent to the EAM-like metal potentials. In recent years the Tersoff-like bond order potential formulation has indeed also been successfully applied to a variety of metals, such as Pt [19], W [20],

Fe [21], Zn [22], and Be [23]. Since bond order potentials can be used for both types of bonding, it is a convenient choice for simulations of mixed covalent-metallic systems.

One such material that has been subject of substantial research is gold nanoparticles and nanorods in a dielectric matrix. The surface plasmon resonance at the gold-dielectric interface gives rise to interesting optical properties that have been utilized in biomedical imaging [24,25] and nanophotonics [26,27].

In a different area of materials science, many studies have focused on swift heavy ion irradiation of gold nanoparticles in silica, since it was found that this treatment leads to shape transformation of the nanoparticles [28–30]. The cause of the shape transformation is still under investigation, and molecular dynamics simulations [31] may provide some answers.

In this work, we develop a bond order potential for gold as a first step to make a bond order description of gold interfaces with covalent materials possible. We test the potential by simulating the size dependent melting of gold nanoclusters.

## 2 Methods

### 2.1 Potential development

We follow the potential fitting methodology for bond order potentials described earlier in e.g. references [19,32]. In the Tersoff-Brenner formalism [18], using the Albe notation [32], the total potential energy is given as a sum of the individual bond energies:

$$E = \sum_{i>j} f_{ij}(r_{ij}) \left[ V_{ij}^R(r_{ij}) - \frac{B_{ij} + B_{ji}}{2} V_{ij}^A(r_{ij}) \right]. \quad (1)$$

<sup>a</sup> e-mail: marie.backman@helsinki.fi

The pair terms describing attractive and repulsive interactions are given by

$$\begin{aligned} V^R(r) &= \frac{D_0}{S-1} \exp[-\beta\sqrt{2S}(r-r_0)], \\ V^A(r) &= \frac{SD_0}{S-1} \exp[-\beta\sqrt{2/S}(r-r_0)], \end{aligned} \quad (2)$$

where  $D_0$  is the dimer bond energy,  $r_0$  the dimer bond distance, and  $S$  an adjustable parameter which determines the slope of the Pauling plot (Eq. (8)). For computational efficiency, the range of the potential is limited to nearest neighbours by the cut-off function

$$f^c(r) = \begin{cases} 1, & r \leq R-D, \\ \frac{1}{2} - \frac{1}{2} \sin\left(\frac{\pi}{2}(r-R)/D\right), & |R-r| \leq D, \\ 0, & r \geq R+D, \end{cases} \quad (3)$$

where  $D$  and  $R$  are adjustable parameters. The bond-order parameter  $B_{ij}$  includes three-body terms and angular dependence

$$\begin{aligned} B_{ij} &= (1 + \chi_{ij})^{-1/2} \quad (4) \\ \chi_{ij} &= \sum_{k(\neq i,j)} f_{ik}^c(r_{ik}) g_{ik}(\theta_{ijk}) \exp[2\mu_{ik}(r_{ij} - r_{ik})]. \end{aligned} \quad (5)$$

The three indices monitor the type dependence of the parameters. The angular function  $g(\theta)$  is given by

$$g(\theta) = \gamma \left( 1 + \frac{c^2}{d^2} - \frac{c^2}{d^2 + (h + \cos\theta)^2} \right). \quad (6)$$

Here  $\gamma$ ,  $c$ ,  $d$ , and  $h$  are adjustable parameters.

The present formalism includes ten free parameters, of which some can be deduced from known properties of the material. The parameter  $\beta$  in equation (2) is determined from the dimer bond energy  $D_0$  and the ground-state oscillation frequency  $\omega$  according to

$$\beta = \frac{2\pi\omega}{\sqrt{2D_0/\mu}}, \quad (7)$$

where  $\mu$  is the reduced mass. The empirically derived Pauling relation gives the bond energy as a function of bond distance,

$$E_b = -D_0 \exp[-\beta\sqrt{2S}(r_b - r_0)]. \quad (8)$$

A plot of  $\ln(E_b)$  as a function of  $r_b$  for different known atomic coordinations of the material should thus follow a straight line with slope  $S$ .

While initial guesses for  $D_0$ ,  $r_0$ ,  $S$ , and  $\beta$  were extracted from empirical data as described above, these parameters were also varied in order to give the best possible fit. To find the remaining parameters of the potential, the functions were fit to experimental and ab initio data for cohesive energies and lattice parameters of the diamond, simple cubic, body-centered cubic, and face-centered cubic structures. All data for the non-ground state structures are from electronic structure calculations

**Table 1.** Bond order potential parameters.

Parameter	Value
$D_0$ (eV)	2.302
$r_0$ (Å)	2.463316
$\beta$ (Å <sup>-1</sup> )	1.586426
$S$	1.95
$\gamma$	$6.374494 \times 10^{-4}$
$c$	3.351525
$d$	0.1649262
$h$	0.9941884
$2\mu$	2.05
$R$ (Å)	3.2
$D$ (Å)	0.2
$b_f$	12
$r_f$	1.7

by Järvi et al. [11]. For the ground state face-centered cubic phase, elastic constants were also included in the fitting routine. Once the mentioned structural properties were described well we further optimized the parameter set to obtain reasonable melting temperature and vacancy formation energy. The derived parameters are given in Table 1.

In order to obtain a more accurate description of atomic interactions at short separations, we modified the repulsive part of the potential to follow the Ziegler-Biersack-Littmark universal repulsive potential [33] at such distances. The modified repulsive potential has the form

$$V_{mod}^R(r) = V^{ZBL}(r)[1 - F(r)] + V^R(r)F(r),$$

where  $V^R$  is the potential for states close to equilibrium described earlier, and the Fermi function is

$$F(r) = \frac{1}{1 + \exp[-b_f(r - r_f)]}.$$

The value of the constants  $b_f$  and  $r_f$  are chosen such that the equilibrium properties are unaffected, and that a smooth fit between  $V^R$  and  $V^{ZBL}$  with no spurious minima is achieved. The obtained parameters are given in Table 1.

## 2.2 Bulk properties

The MD simulation code PARCAS [34]<sup>1</sup> was used to test the developed potential. Properties including threshold displacement energy, melting temperature, surface energy, and defect energies were investigated.

We determined the threshold displacement energy in simulations using the box size  $10 \times 10 \times 14$  unit cells at

<sup>1</sup> The main principles of the molecular dynamics algorithms are presented in [46,47]. The adaptive time step and electronic stopping algorithms are the same as in [48].

10 K. A random atom was given kinetic energy in a random direction and the energy was increased in increments of 2 eV until a stable defect was formed. We used the definition for the average displacement threshold used by Nordlund et al. in reference [35]. In defining values for the crystal directions a 20° spreading of the angle was included to account for beam spreading in experiments.

The bulk melting temperature was determined from a simulation of a molten phase in contact with a crystalline phase. Below the melting temperature the molten phase crystallizes and above it the crystalline phase starts to melt. We obtained a bulk melting temperature of 1640 K, somewhat higher than the literature value of 1337.33 K [36].

We performed 5 ns long simulations of the diffusion of a self-interstitial at different temperatures. The diffusion coefficient was calculated from the mean square displacement of interstitials using the Einstein relation. A least square fit to an Arrhenius plot of the obtained diffusion coefficients gave us the self-interstitial migration energy.

We studied the surface energies at 0 K of the (111), (110), and (100) surfaces by comparing the potential energy of the free surface to that of the bulk.

### 2.3 Nanoparticle melting simulations

We used the developed analytical potential to simulate the size dependent melting temperature of gold nanoclusters in vacuum [37]. From fcc crystals with the bulk lattice constant of gold, we created spherical nanoclusters with diameters between 2 and 18 nm. To determine the melting temperature the nanoclusters were equilibrated for 1 ns at different temperatures using Berendsen temperature control [38]. In case the potential energy had not stabilized after 1 ns, a longer simulation time was used. The heated nanoclusters were inspected visually and analyzed with a structure factor analysis method used in reference [39] for the same purpose. When at some temperature the average structure factor, visual inspection, and potential energy all indicated complete melting, the nanocluster was considered molten.

The bulk melting or condensation temperature can only be determined accurately if there is a seed for melting or crystallization, respectively, from which the phase transformation can nucleate. If no such seed is present, superheating or supercooling occurs. For this reason we use a two-phase simulation to determine the bulk melting temperature of the potential (see above). In nanoclusters the free surface area acts as nucleation site for melting, hence, superheating is avoided as long as the surface-to-volume ratio is high.

## 3 Results and discussion

In Table 2 the cohesive energies, lattice parameters, and elastic constants obtained from the bond order potential are compared to the reference data from experiments and

**Table 2.** Comparison of properties of dimer and bulk phases between the literature and the developed bond order potential.  $E_{coh}$ : cohesive energy (eV/atom);  $r_0$ : dimer bond length (Å);  $\omega$ : ground state oscillation frequency ( $\text{cm}^{-1}$ );  $a_0$ : lattice parameter (Å);  $B$ : bulk modulus (GPa);  $B'$ : pressure derivative of bulk modulus;  $c_{ij}$ : elastic constants (GPa);  $T_{melt}$ : melting temperature (K);  $E_{vac}^f$ : vacancy formation energy (eV);  $E_{int}^f$ : interstitial formation energy (eV);  $E_{int}^m$ : self-interstitial migration energy (eV);  $E_d$ : average threshold displacement energy (eV);  $\gamma$ : surface energy ( $\text{J}/\text{m}^2$ ). The properties are measured at 0 K unless otherwise specified.

	Literature	BOP
<b>Dimer</b>		
$E_{coh}$	-1.151 [40]	-1.151
$r_0$	2.472 [40]	2.463
$\omega$	191 [40]	179
<b>DIA</b>		
$E_{coh}$	-2.80 [11]	-2.60
$a_0$	5.98 [11]	6.11
<b>SC</b>		
$E_{coh}$	-3.53 [11]	-3.34
$a_0$	2.68 [11]	2.69
<b>BCC</b>		
$E_{coh}$	-3.77 [11]	-3.67
$a_0$	3.23 [11]	3.17
<b>FCC</b>		
$E_{coh}$	-3.81 [49]	-3.81
$a_0$	4.065 [49]	4.065
$B$	180 [50]	168
$B'$	5.5 [51]	5.5
$c_{11}$	192 [36], at room temperature.	201
$c_{12}$	163 [36], at room temperature.	151
$c_{44}$	42 [36], at room temperature.	47
$T_{melt}$	1337.3 [36]	1640
$E_{vac}^f$	0.89 [8,52]	0.80
$E_{int}^f$		4.41
$E_{int}^m$		0.11
$E_d$	44 [53]	47
$E_d^{100}$		24
$E_d^{110}$		52
$E_d^{111}$		28
$\gamma_{111}$		0.67
$\gamma_{100}$	1.50 [54], average surface energy.	0.90
$\gamma_{110}$		0.97
$\gamma_{110}^{\text{missing row}}$		0.86

ab initio calculations. The analytic potential shows good agreement with established literature values.

Interstitials have not been observed experimentally in gold [40], possibly because of a very low migration energy [41,42]. The ground state structure of interstitials in gold is hence not known. With the present potential we observe that a single interstitial gives rise to a crowdion in the [111] direction with formation and migration energy given in Table 2. This suggests that crowdion motion might explain the very low migration energy in experiments.



**Fig. 1.** Cross-section of an 18 nm nanocluster melting from the surface inward.

The surface energies are underestimated, but on par with the values obtained with the commonly used Foiles-Baskes EAM potential for gold [1,2]. (The second value for the (110) surface energy in Tab. 2 refers to the  $(1 \times 2)$  missing row reconstruction found in gold [43].) Some newer potentials report surface energies that are in better agreement with experimental data, see for instance [11] and [13], where the former includes a comparison of surface energies for different gold potentials. It should be noted that the low surface energies for the developed potential is a consequence of not fitting to surface properties rather than a fundamental weakness of the potential formalism.

As previously shown by for instance Lewis et al. [44], simulations of gold nanocluster melting reveal that melting begins at the surface and proceeds inward. This is illustrated in Figure 1. Small clusters are observed to transform from spherical to faceted clusters at elevated temperatures (see Fig. 2).

The nanoclusters are found to exhibit size dependent melting temperature, in accordance with thermodynamic theory and a vast array of literature (see e.g. Ref. [45] and references therein). Figure 3 shows the ratio of nanocluster to bulk melting temperature for the simulated nanocluster sizes. This ratio approaches unity as the nanocluster diameter increases. Compared to experiments by Buffat and Borel [37], the nanocluster-to-bulk melting temperature ratio found in both our simulations and the simulations by Lewis is higher. The simulations are performed with perfect crystalline clusters where the only seed for melting is the surface, therefore, superheating may explain this discrepancy. We find that the bulk melting temperature is not reached even for the largest nanocluster simulated.

## 4 Conclusions

An analytic bond order potential for gold was developed to make development of gold-covalent interface potentials possible. The potential provides a good description of bulk properties, such as cohesive energy, lattice parameter and elastic constants, while the surface energies are underestimated. The melting temperature is within reasonable range from the literature value and the size dependence



**Fig. 2.** A gold nanocluster of diameter 6 nm (a) before melting, (b) at the onset of melting, and (c) after melting. Note the transition from spherical cluster in (a) to faceted at elevated temperatures in (b).

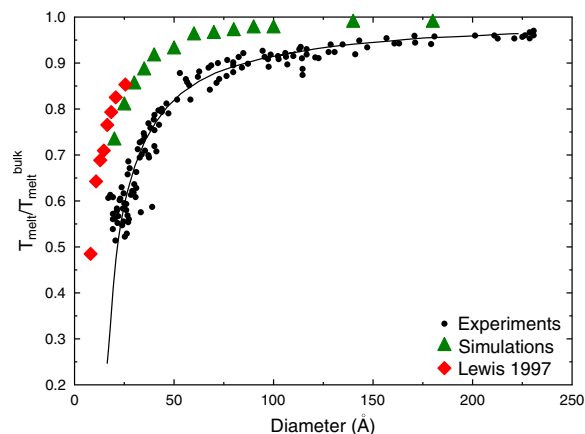


**Fig. 3.** Relative melting temperature as a function of cluster diameter, compared to experimental results by Buffat and Borel [37] and MD simulations by Lewis et al. [44].

of gold nanocluster melting temperatures is reproduced qualitatively.

Computing time was provided by the Newton HPC Program at the University of Tennessee.

## References

1. S.M. Foiles, M.I. Baskes, M.S. Daw, *Phys. Rev. B* **33**, 7983 (1986)
2. S.M. Foiles, M.I. Baskes, M.S. Daw, *Phys. Rev. B* **37**, 10378 (1988)
3. J. Cai, Y.Y. Ye, *Phys. Rev. B* **54**, 8398 (1996)
4. G. Grochola, S.P. Russo, I.K. Snook, *J. Chem. Phys.* **123**, 204719 (2005)
5. F. Ercolessi, M. Parrinello, E. Tosatti, *Phil. Mag. A* **58**, 213 (1988)
6. S.B. Sinnott, M.S. Stave, T.J. Raeker, A.E. DePristo, *Phys. Rev. B* **44**, 8927 (1991)
7. F. Cleri, V. Rosato, *Phys. Rev. B* **48**, 22 (1993)
8. G.C. Kallinteris, N.I. Papanicolaou, G.A. Evangelakis, D.A. Papaconstantopoulos, *Phys. Rev. B* **55**, 2150 (1997)
9. H. Chamati, N.I. Papanicolaou, *J. Phys.: Condens. Matter* **16**, 8399 (2004)
10. L.M. Molina, J.A. Alonso, *J. Phys. Chem. C* **111**, 6668 (2007)
11. T.T. Järvi, A. Kuronen, M. Hakala, K. Nordlund, A.C.T. van Duin, W.A. Goddard III, T. Jacob, *Eur. Phys. J. B* **66**, 75 (2008)
12. J.A. Keith, D. Fantauzzi, T. Jacob, A.C.T. van Duin, *Phys. Rev. B* **81**, 235404 (2010)
13. S. Olivier, R. Conte, A. Fortunelli, *Phys. Rev. B* **77**, 054104 (2008)
14. G.C. Abell, *Phys. Rev. B* **31**, 6184 (1985)
15. J. Tersoff, *Phys. Rev. B* **37**, 6991 (1988)
16. D.W. Brenner, *Phys. Rev. B* **42**, 9458 (1990)
17. D.W. Brenner, *Phys. Rev. B* **46**, 1948 (1992)
18. D.W. Brenner, *Phys. Rev. Lett.* **63**, 1022 (1989)
19. K. Albe, K. Nordlund, R.S. Averback, *Phys. Rev. B* **65**, 195124 (2002)
20. N. Juslin, P. Erhart, P. Träskelin, J. Nord, K.O.E. Henriksson, K. Nordlund, E. Salonen, K. Albe, *J. Appl. Phys.* **98**, 123520 (2005)
21. M. Müller, P. Erhart, K. Albe, *J. Phys.: Condens. Matter* **19**, 326220 (2007)
22. P. Erhart, N. Juslin, O. Goy, K. Nordlund, R. Müller, K. Albe, *J. Phys.: Condens. Matter* **18**, 6585 (2006)
23. C. Björkas, N. Juslin, H. Timkó, K. Vörtler, K. Nordlund, K.O.E. Henriksson, P. Erhart, *J. Phys.: Condens. Matter* **21**, 445002 (2009)
24. D. Yelin, D. Oron, S. Thiberge, E. Moses, Y. Silberberg, *Opt. Express* **11**, 1385 (2003)
25. I.H. El-Sayed, X. Huang, M.A. El-Sayed, *Nano Lett.* **5**, 829 (2005)
26. S. Link, M.A. El-Sayed, *Annu. Rev. Phys. Chem.* **54**, 331 (2003)
27. Q.H. Wei, K.H. Su, S. Durant, X. Zhang, *Nano Lett.* **4**, 1067 (2004)
28. K. Awazu, X. Wang, M. Fujimaki, J. Tominaga, H. Aiba, Y. Ohki, T. Komatsubara, *Phys. Rev. B* **78**, 054102 (2008)
29. P. Kluth, R. Giulian, D.J. Sprouster, C.S. Schnohr, A.P. Byrne, D.J. Cookson, M.C. Ridgway, *Appl. Phys. Lett.* **94**, 113107 (2009)
30. E.A. Dawi, G. Rizza, M.P. Mink, A.M. Vredenberg, F.H.P.M. Habraken, *J. Appl. Phys.* **105**, 074305 (2009)
31. A.A. Leino, O.H. Pakarinen, F. Djurabekova, K. Nordlund, *Nucl. Instrum. Methods Phys. Res. B* **282**, 76 (2011)
32. K. Albe, K. Nordlund, J. Nord, A. Kuronen, *Phys. Rev. B* **66**, 035205 (2002)
33. J.F. Ziegler, J.P. Biersack, U. Littmark, *The Stopping and Range of Ions in Matter* (Pergamon, New York, 1985)
34. K. Nordlund, *PARCAS Computer Code* (2006), <http://link.aps.org/doi/10.1103/PhysRevB.85.024105>
35. K. Nordlund, J. Wallenius, L. Malerba, *Nucl. Instrum. Methods Phys. Res. B* **246**, 322 (2005)
36. *CRC Handbook of Chemistry and Physics, Internet Version*, edited by D.R. Lide, 92nd edn. (Taylor and Francis, 2012)
37. P. Buffat, J.P. Borel, *Phys. Rev. A* **13**, 2287 (1976)
38. H.J.C. Berendsen, J.P.M. Postma, W.F. van Gunsteren, A. DiNola, J.R. Haak, *J. Chem. Phys.* **81**, 3684 (1984)
39. J.A. Pakarinen, M. Backman, F. Djurabekova, K. Nordlund, *Phys. Rev. B* **79**, 085426 (2009)
40. P. Pyykkö, *Angew. Chem. Int. Ed.* **43**, 4412 (2004)
41. R.C. Birtcher, W. Hertz, G. Fritsch, J.E. Watson, *Proc. Intl. Conf. on Fundamental Aspects of Radiation Damage in Metals, CONF-751006-P1* (1975), Vol. 1, p. 405
42. H. Schroeder, B. Stritzker, *Radiation effects* **33**, 125 (1977)
43. G. Binnig, H. Rohrer, C. Gerber, E. Weibel, *Surf. Sci. Lett.* **131**, L379 (1983)
44. L.J. Lewis, P. Jensen, J.L. Barrat, *Phys. Rev. B* **56**, 2248 (1997)
45. F. Baletto, R. Ferrando, *Rev. Mod. Phys.* **77**, 371 (2005)
46. K. Nordlund, M. Ghaly, R.S. Averback, M. Caturla, T. Diaz de la Rubia, J. Tarus, *Phys. Rev. B* **57**, 7556 (1998)
47. M. Ghaly, K. Nordlund, R.S. Averback, *Phil. Mag. A* **79**, 795 (1999)
48. K. Nordlund, *Comput. Mater. Sci.* **3**, 448 (1995)
49. Y. Kimura, Y. Qi, T. Cagin, W.A. Goddard III, *MRS Symposium Ser.* **554**, 43 (1999)
50. O.L. Anderson, D.G. Isaak, S. Yamamoto, *J. Appl. Phys.* **65**, 1534 (1989)
51. K. Takemura, A. Dewaele, *Phys. Rev. B* **78**, 104119 (2008)
52. H.E. Schaefer, *Phys. Stat. Sol. A* **102**, 47 (1987)
53. P. Jung, *Phys. Rev. B* **23**, 664 (1981)
54. W.R. Tyson, W.A. Miller, *Surf. Sci.* **62**, 267 (1976)